Chemical Science

EDGE ARTICLE

View Article Online
View Journal | View Issue

Cite this: *Chem. Sci.*, 2019, **10**, 10925

All publication charges for this article have been paid for by the Royal Society of Chemistry

Trapping an unprecedented Ti_3C_3 unit inside the icosahedral C_{80} fullerene: a crystallographic survey†

Pengyuan Yu,‡ Wangqiang Shen,‡ Lipiao Bao,‡ Changwang Pan, Zdenek Slanina and Xing Lu *

The sub-nanometer cavity of fullerene cages is an ideal platform to accommodate otherwise unstable species for accurate structural characterization with, for example, rather accurate single crystal X-ray diffraction (XRD) crystallography. Herein, we report the successful entrapment of an isolated Ti_3C_3 moiety inside the icosahedral-C_{80} cage to form $Ti_3C_3@I_h$-C_{80} *via* an arc-evaporation process in the gas phase. The single crystal XRD crystallographic results unambiguously reveal that the C_3-unit adopts an unprecedented cyclopropane-like structure which coordinates with the three titanium atoms in an unexpected fashion where the triangular C_3-unit is nearly perpendicular to the Ti_3-plane. The intercalation of a cyclopropanated C_3-unit into the titanium layer is thus unambiguously confirmed. The theoretical results reveal that the Ti_3C_3 cluster transfers six electrons to the I_h-C_{80} cage so that each titanium atom has a positive charge slightly above +2 and the C_3-unit is negatively charged with about −1. It is noteworthy that this is the first observation of the cyclopropane-coordination fashion in any reported organometallic complex, providing new insights into coordination chemistry.

Received 27th August 2019
Accepted 14th October 2019

DOI: 10.1039/c9sc04315b

rsc.li/chemical-science

Introduction

Fullerene cages serve as a protector to host a variety of isolated metal atom(s) or otherwise unstable metallic units to form so-called endohedral metallofullerenes (EMFs). By virtue of the solubility of EMFs, high-quality single crystals can be obtained and thus the interplay between the metallic species within the clusters, in addition to the metal–cage interactions, is possible to study by the sophisticated single crystal X-ray diffraction (XRD) approach. Up to now, a collection of EMFs containing one to three pure metal atoms, which are called mono-, di- and tri-EMFs, respectively, has been crystallographically confirmed.[1–4] Interesting results such as direct bonding between the repulsive metal ions (*e.g.*, Lu^{2+}–Lu^{2+}, U^{3+}–U^{3+} or Y^{2+}–Y^{2+}) have been achieved taking advantage of the confinement effect of the fullerene cages.[5–7]

In addition, various metallic clusters, such as metal nitride,[8] carbide,[9] oxide,[10] sulfide[11] and even cyanide,[12] have been successfully trapped inside fullerene cages. It is noteworthy that only with the protection of the fullerene cages are the metallic clusters able to exist and they transfer a certain number of electrons to the surrounding cages. As typical examples, an improbable monometallic cluster YCN[12] was found in $C_s(6)$-C_{82} featuring a two-electron-transfer configuration but the I_h-C_{80} is able to host a variety of metallic species such as La_2,[13] Sc_3N,[8] Sc_3C_2,[14] Sc_4C_2,[15] $TiSc_2C_2$,[16] $TiDy_2C$,[17] Sc_3CH[18] and Sc_3C_2CN[19] which donate six electrons to the cage. It's noted that encapsulation of a carbide cluster consisting of either an odd or an even number of carbon atoms is feasible. Impressively, Popov *et al.* theoretically revealed $Sc_4C_3@C_{80}$ encapsulating a triangular aromatic C_3 cluster with two pairs of Sc atoms coordinating with the C_3 moiety.[20] Recently, Chen and coworkers[21] reported the structure of $U_2C@C_{80}$ where a non-bridged uranium-carbon double bond was identified. More interestingly, Popov and coworkers[22] reported that a titanium–carbon double bond (Ti=C) exists in $TiLu_2C@I_h$-C_{80}, representing the first example of EMFs with a multiple bond between the metal and the non-metal atom of the endohedral cluster. It is thus expected that novel and even unprecedented bonding features are possibly observed in EMFs containing different metallic clusters.

Herein, we report the preparation and systematic characterization of a brand-new titanium-containing EMF, namely $Ti_3C_3@I_h$-C_{80}, which is one of the rare examples of EMFs that do not contain group-III elements. X-ray crystallographic results reveal that the C_3-unit of the Ti_3C_3 cluster resembles cyclopropane with an average C–C distance of 1.380 Å, perpendicularly

State Key Laboratory of Materials Processing and Die & Mould Technology, School of Materials Science and Engineering, Huazhong University of Science and Technology, 1037 Luoyu Road, Wuhan, 430074 China. E-mail: lux@hust.edu.cn

† Electronic supplementary information (ESI) available. CCDC 1883920. For ESI and crystallographic data in CIF or other electronic format see DOI: 10.1039/c9sc04315b

‡ These authors contributed equally to this work.

coordinated with the Ti_3-moiety, exhibiting a totally unexpected coordination fashion in organometallic chemistry.

Results and discussion

Soot containing titanium-EMFs was synthesized by an arc discharge method using TiC as the precursor. $SnCl_4$ was first chosen to react with the extract for the enrichment of Ti-EMFs followed by multiple-stage HPLC separation to obtain a pure sample of $Ti_3C_3@C_{80}$ (Fig. S1 and S2†). Its MALDI-TOF mass spectrum shows a single peak at m/z 1139.8 (Fig. 1a) which is perfectly consistent with the calculated results of Ti_3C_{83}. Interestingly, the retention time of $Ti_3C_3@I_h$-C_{80} in a Buckyprep column is much longer than that of $Sc_3N@I_h$-C_{80} (Fig. S3†). Previous studies have suggested a correlation between the HPLC retention time and the molecular geometry of fullerenes.[23] Generally, the retention mechanism is proportional to the cage polarizability and is dominated by π–π interactions with the stationary phase. This phenomenon may suggest a different electronic configuration of the title compound from that of $Sc_3N@I_h$-C_{80}. Consistently, the absorption spectrum of $Ti_3C_3@I_h$-C_{80} (Fig. 1b) shows a small bandgap of 0.82 eV (onset at 1500 nm) in comparison with the large one of $Sc_3N@I_h$-C_{80} (1.70 eV),[24] suggesting a relatively low stability and unique electronic configuration of $Ti_3C_3@I_h$-C_{80}. In addition, no signal is observed in the EPR spectrum of $Ti_3C_3@I_h$-C_{80} even at 100 K (Fig. S4†), indicative of its diamagnetic property with a closed-shell electronic configuration. Compared to the previously reported Ti-containing mixed-metal EMFs, such as $TiSc_2N@I_h$-C_{80} (ref. 25) and $TiY_2N@C_{80}$,[26] which feature obvious EPR signals at low temperatures, it can be concluded that our title compound has a different electronic structure, which is presumably attributed to the difference in the spin distribution of the embedded clusters.

The structure of Ti_3C_{83} is unambiguously established as $Ti_3C_3@I_h$-C_{80}, instead of any other form such as $Ti_3C@C_{82}$, by a single crystal XRD study performed on a black crystal obtained by slow diffusion of a benzene solution of Ni^{II}(OEP) (OEP is the dianion of octaethyl porphyrin) into the CS_2 solution of the EMF. The $Ti_3C_3@I_h$-$C_{80}\cdot Ni^{II}(OEP)\cdot 2C_6H_6$ cocrystal falls into the monoclinic $C2/m$ space group, where a half of Ni^{II}(OEP) and a half of $Ti_3C_3@I_h$-C_{80} are included in its asymmetric unit cell. The crystallographic mirror plane coincides with one of the symmetric planes of the I_h-C_{80} cage, resulting in a fully ordered I_h-C_{80} cage by combining the existing half with its mirror image.

Inside the cage, disorder is observed for the Ti_3C_3 cluster (see ESI Fig. S5 and Table S1 for details†). Specifically, one carbon atom in the C_3-unit exhibits two disordered positions generated by the crystallographic mirror plane, whereas the other two located in the crystallographic mirror plane are fully ordered. Eleven Ti sites are distinguished for the three titanium atoms with occupancy values ranging from 0.127 to 0.506. In fact, three of the disordered sites apart from Ni^{II}(OEP) belong to one Ti atom, with Ti2 as the major one (occupancy = 0.505). Meanwhile, two major sites out of the remaining eight disordered Ti-positions close to Ni^{II}(OEP), namely Ti1 and Ti1A (occupancy = 0.506), can be assigned to the other two Ti atoms.

Fig. 2 displays the molecular structures of $Ti_3C_3@I_h$-C_{80} showing only the major metal site together with the co-crystallized Ni^{II}(OEP) molecule. The porphyrin moiety nestles the

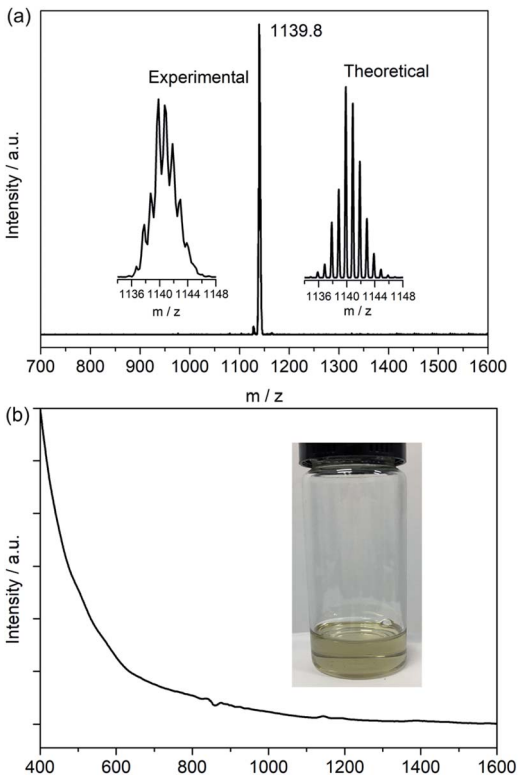

Fig. 1 (a) MALDI-TOF mass spectrum of purified $Ti_3C_3@I_h$-C_{80}. The insets show the experimental and theoretical isotopic distributions of Ti_3C_{83}. (b) Vis-NIR absorption spectrum of $Ti_3C_3@I_h$-C_{80} recorded in CS_2. A photograph of the corresponding solution is shown in the inset.

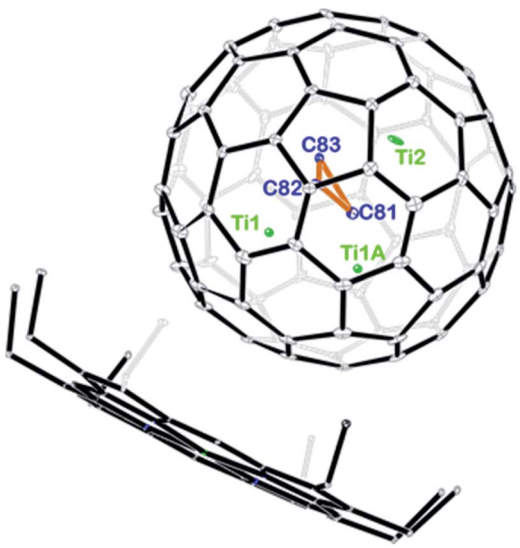

Fig. 2 ORTEP drawing of $Ti_3C_3@I_h$-$C_{80}\cdot$[Ni^{II}(OEP)] with 15% thermal ellipsoids. Only the major Ti_3C_3 site is shown. Solvent molecules and H atoms are omitted for clarity.

fullerene cage with the shortest Ni–cage–carbon distance of 2.950 Å, suggesting substantial π–π interactions. Interestingly, the three carbon atoms stay in the center of the cage to form cyclopropane with an average bond length of 1.380 Å. The Ti–Ti distances among the three titanium atoms are 2.976 Å for Ti1–Ti1A and 3.604 Å for Ti1–Ti2 and Ti1A–Ti2, respectively, which are comparable to the values observed in organotitanium complexes, indicating weak metal–metal interactions between the titanium atoms.[27–29] From a geometric point of view, the three titanium atoms intercalate between the cage and the C_3-unit, preventing the encapsulated carbon atoms from being merged with the cage framework.

Fig. 3 illustrates the configuration of the major Ti_3C_3 site showing its relationship to the adjacent cage frameworks. Each titanium atom is centered above a respective [5,6]-ring junction with average Ti–C (cage) distances of 2.12, 2.12, and 2.13 Å, respectively, which fall in the range of typical Ti–C single bond lengths in reported organotitanium compounds (usually 2.1 Å),[30,31] suggestive of strong metal–cage interactions (see also Table S2, ESI†). In contrast, the Ti–C distances within the Ti_3C_3 cluster are spread in a wide range from 1.838 Å to 3.090 Å, indicative of a rather complicated coordination environment. Interestingly, the plane of the C_3-unit is nearly perpendicular to that of the Ti_3-moiety with a dihedral angle of 83.43°, presenting a unique coordination fashion between carbon and titanium. To the best of our knowledge, such an unusual coordination pattern for cyclopropane interacting with metal ions has never been reported in any organometallic complexes, despite the above-mentioned theoretical possibility of a triangular C_3 unit inside the $Sc_4C_3@C_{80}$.[20]

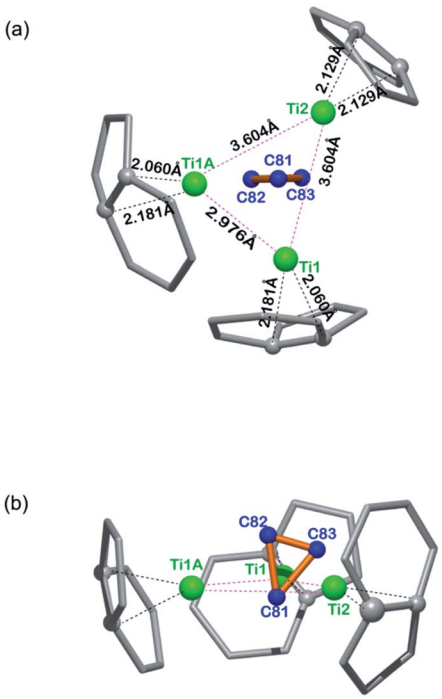

Fig. 3 Orthogonal views showing the relative position of the major Ti_3C_3 site to the closest cage portions.

We have performed density functional theory (DFT) calculations at the B3LYP/3-21G∼SSD level to understand the unique coordination environment in $Ti_3C_3@I_h$-C_{80}. The calculated Wiberg indices for the bonds in the cyclopropane ring are 1.18, 0.80, and 0.75 while their calculated lengths are 1.39 Å, 1.58 Å, and 1.62 Å, respectively, a bit longer than the corresponding X-ray results. As for the Ti_3-unit, there are six bond indices between the ring carbons and Ti atoms larger than 0.5, namely 0.88, 0.67, 0.64, 0.60, 0.59, and 0.58. There is one (weak) C–C double bond not bridged by Ti, one (weak) single bond bridged by one Ti, and one (still weaker) single bond bridged by two Ti atoms. In this simplified picture (Fig. 4a), each Ti atom is bonded to the ring *via* two Ti–C bonds, supporting the results of the geometry of the embedded Ti_3C_3 cluster (Fig. 4b) obtained by the single crystal X-ray method. Moreover, the electron distribution in $Ti_3C_3@I_h$-C_{80} is visualized in Fig. S6, ESI† for more graphical information about bonds between the carbons of the cage and also bonds in the encapsulate, showing a selected isosurface of electron density (*i.e.*, every point of the surface has the same prescribed value of the electron density). At the selected constant electron density of 0.086 a.u., the bonds in the cage and especially in the Ti_3C_3 cluster are rather well visible, where the near-vertical coordination environment of the Ti_3-unit and C_3-unit was found. Such a clear picture further provides us with unique bonding information. The B3LYP/3-21G∼SDD Mulliken charges in $Ti_3C_3@I_h$-C_{80} on Ti atoms are 2.77, 2.48, and 2.44 while on the ring carbons they are −0.49, −0.41, and −0.22. The Mulliken-charge choice is supported[32] by the fact that it is in good agreement with the available observed charges[33] for metallofullerenes. However, unless there are charges deduced from observations for a class of clusterfullerenes, it cannot really be decided which particular charge definition is the best[34] for the class. Thus, the results for the isolated $Ti_3C_3@I_h$-C_{80} system demonstrate a charge transfer of about six electrons to the cage, matching the charge state of common $(I_h$-$C_{80})^{6-}$ reflected by the Vis-NIR spectrum.

Theoretically, the Ti_3C_3 encapsulation is also favorable from the calculated energetics point of view.[35] The B3LYP/6-31G*∼SDD encapsulation-energy gain per one encapsulated atom for $Ti_3C_3@I_h$-C_{80} is calculated to be about 18 kcal per mol per atom which is even larger than a relative energy gain computed for the recently isolated $Y_2C_2@C_1(1660)$-C_{108}.[36] The

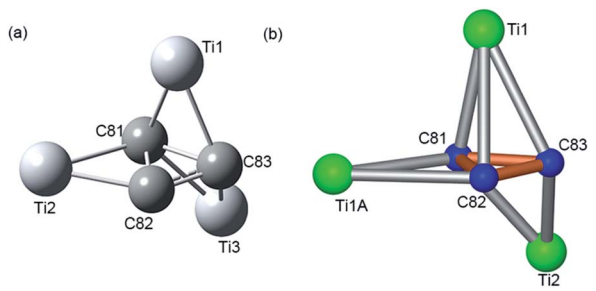

Fig. 4 (a) The optimized Ti_3C_3 configuration at the B3LYP/3-21G∼SDD level and (b) geometry configuration of the major site of the Ti_3C_3 cluster from X-ray results.

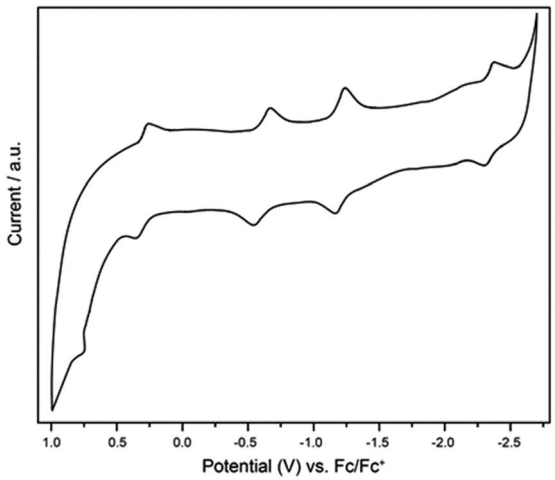

Fig. 5 CV curve of Ti_3C_3@I_h-C_{80}. Conditions: working electrode, glassy carbon electrode; counter electrode, Pt wire; reference electrode, Ag wire; supporting electrolyte, 0.05 M $TBAPF_6$ in *o*-DCB with ferrocene as the internal standard. Scan rate: 100 mV s^{-1}.

stability calculations indeed support the finding that a novel EMF containing a unique Ti_3C_3 cluster was experimentally obtained.

The electrochemical properties of Ti_3C_3@I_h-C_{80} were measured in *o*-dichlorobenzene (*o*-DCB) by cyclic voltammetry (CV) and the profile is shown in Fig. 5. In the anodic region, Ti_3C_3@I_h-C_{80} displays a reversible oxidation step at 0.30 V and an irreversible one at 0.77 V whereas in the cathodic region, three reversible reduction steps are observed at −0.62 V, −1.22 V and −2.31 V. The electrochemical gap is thus calculated to be 0.92 V which is quite smaller than those of the other I_h-C_{80} based Ti-containing EMFs, namely, $TiLu_2C$@I_h-C_{80} (ref. 22), $TiSc_2C_2$@I_h-C_{80} and $TiSc_2C$@I_h-C_{80},[16] suggesting a lower kinetic stability of Ti_3C_3@I_h-C_{80} which is also consistent with the Vis-NIR result. In addition, the irreversible oxidation process of Ti_3C_3@I_h-C_{80} has not been reported for the other Ti-based EMFs[4,17,22,26] (Table 1). These results suggest that we can tune the electronic properties of Ti-EMFs by varying the number of redox-active Ti atoms. Furthermore, the frontier molecular orbital of Ti_3C_3@I_h-C_{80} visualized in Fig. S7 (ESI†) shows that the predominant localization of the LUMO is on the Ti_3C_3 cluster (mainly on the Ti atoms), suggesting that the first reduction step is ascribed to the alteration of the reduction behavior of the inner cluster, similar to the case of Sc_2TiC_2@I_h-C_{80}.[27]

Table 1 Redox potentials of Ti_3C_3@I_h-C_{80} and typical Ti-based EMFs[a]

EMFs	$^{ox}E_2$	$^{ox}E_1$	$^{red}E_1$	$^{red}E_2$	$^{red}E_3$	ΔE_{gap}[b]	Ref.
Ti_3C_3@I_h-C_{80}	0.77[c]	0.30	−0.62	−1.22	−2.31	0.92	*This work*
$TiLu_2C$@I_h-C_{80}	—	0.64	−0.91	—	—	1.55	22
$TiSc_2C$@I_h-C_{80}	—	0.66	−0.67	−1.51	−1.66	1.33	16
Sc_2TiC_2@I_h-C_{80}	—	0.53	−0.76	−1.01	−1.96	1.26	16
Dy_2TiC@I_h-C_{80}	—	0.61	−0.97	−1.62	−1.87	1.58	17
Dy_2TiC_2@I_h-C_{80}	—	0.47	−1.14	−1.58	−2.21	1.61	17

[a] Half-cell values in V *versus* $Fe(Cp)_{2+/0}$ unless otherwise noted. [b] $\Delta E_{gap} = {}^{ox}E_1 - {}^{red}E_1$. [c] Irreversible peak value.

Conclusions

An unprecedented Ti_3C_3 cluster has been successfully entrapped inside the I_h-C_{80} cage to form a stable compound. X-ray results reveal a novel coordination fashion by which the cyclopropane-like C_3-unit perpendicularly coordinates to the Ti_3-moiety. The electronic configuration of $(Ti_3C_3)^{6+}$@$C_{80}{}^{6-}$ was confirmed according to the Vis-NIR spectroscopic and electrochemical characterization in addition to DFT calculations. Successful entrapment of the Ti_3C_3 cluster inside fullerene cages and identification of the unprecedented cyclopropane-coordination fashion may stimulate intensive interest in creating new hybrid molecules with fullerenes as protectors and discovering new reactivities in coordination chemistry.

Experimental

Synthesis and isolation of Ti_3C_3@I_h-C_{80}

Soot containing titanium-EMFs was produced by evaporating graphite rods packed with mixed TiC and graphite powder (mole ratio of Ti : C = 1 : 10) under a 400 mbar He atmosphere and 100 A current. The soot was extracted with CS_2, and the filtered extract was treated with $SnCl_4$ for the enrichment of Ti-EMFs, followed by multi-stage HPLC separation conducted on an LC-908 machine (Japan Analytical Industry Co. Ltd.) sequentially employing a 5PBB column (∅ 20 × 250 mm) and a Buckyprep column (∅ 20 × 250 mm). More details about the $SnCl_4$ treatment and HPLC separations are present in the ESI.†

Spectroscopic and electrochemical studies

Matrix-assisted laser desorption/ionization time-of-flight (MALDI-TOF) (MICROFLEX, Bruker, Germany) was used for the mass spectroscopic characterization. The Vis-NIR spectrum was measured on a PE Lambda 750S spectrophotometer in CS_2. Cyclic voltammetry (CV) was performed in *o*-dichlorobenzene using a CHI-660E instrument with 0.05 M $TBAPF_6$ as the electrolyte. The electron paramagnetic resonance (EPR) spectrum of Ti_3C_3@I_h-C_{80} was recorded with a Bruker A300 spectrometer in toluene.

Crystallographic characterization

Cocrystals of Ti_3C_3@I_h-C_{80} were obtained by slow diffusion of a benzene solution of Ni^{II}(OEP) into a CS_2 solution of the EMF in a glass tube at room temperature for one month. Single-crystal X-ray data were collected at 100 K using a radiation wavelength of 0.6525 Å with a MarCCD detector at beamline BL17B of the Shanghai Synchrotron Radiation Facility. A multi-scan method was used for absorption corrections. The structures were solved with direct methods and were refined with SHELXL-2014.[37]

Crystal data of Ti_3C_3@I_h-C_{80}·Ni^{II}(OEP)·2(C_6H_6)

Black block, 0.31 × 0.24 × 0.20 mm, monoclinic, space group $C2/m$, a = 25.0964(9) Å, b = 15.1544(5) Å, c = 19.7269(7) Å, β = 95.3360(10)°, V = 7470.0(5) Å^3, F_w = 1888.20, λ = 0.6525 Å, Z = 4, D_{calc} = 1.679 Mg m^{-3}, μ = 0.498 mm^{-1}, T = 100 K, $R_1[I > 2\sigma(I)]$ =

0.1079, wR_2 (all data) = 0.2972, GOF (on F^2) = 1.068. The maximum residual electron density is 1.953 e Å^{-3}. Crystallographic data have been deposited in the Cambridge Crystallographic Data Center (CCDC number: 1883920).†

Computational study of $Ti_3C_3@I_h$-C_{80}

The structure optimization started with a combined basis set, the standard 3-21G basis[38] for C atoms and SDD basis[39] with the SDD effective core potential for Ti atoms, applied within the density functional theory (DFT) approach, namely using Becke's three parameter functional[40] with the non-local Lee–Yang–Parr correlation functional[41] (denoted as B3LYP/3-21G∼SDD). Herein, analytical harmonic vibrational analysis is then carried out in order to confirm that the local-energy minimum was indeed localized. The B3LYP/3-21G∼SDD optimized structure was further refined by performing re-optimizations with the standard 6-31+G* basis set[42] for C atoms (B3LYP/6-31+G*∼SDD). Moreover, in the latter structure the encapsulation energy[43] (the energy gain upon encapsulation of three Ti and three C atoms into the C_{80} cage) was evaluated at the B3LYP/6-31G*∼SDD level with inclusion of the basis set superposition error[44] (BSSE/CP7) and the so-called steric correction that reflects the cage distortion upon encapsulation.[45] All the computations were carried out with the Gaussian 09 program package.[46]

Conflicts of interest

There are no conflicts to declare.

Acknowledgements

Financial support from the NSFC (51672093, 51602112 and 51602097) is gratefully acknowledged. We thank the staff from the BL17B beamline of the National Center for Protein Science Shanghai at the Shanghai Synchrotron Radiation Facility for assistance during data collection and the Analytical and Testing Center in the Huazhong University of Science and Technology for all related measurements.

Notes and references

1 X. Lu, L. Feng, T. Akasaka and S. Nagase, *Chem. Soc. Rev.*, 2012, **41**, 7723–7760.
2 L. Bao, P. Peng and X. Lu, *Acc. Chem. Res.*, 2018, **51**, 810–815.
3 A. A. Popov, S. Yang and L. Dunsch, *Chem. Rev.*, 2013, **113**, 5989–6113.
4 S. Yang, T. Wei and F. Jin, *Chem. Soc. Rev.*, 2017, **46**, 5005–5058.
5 W. Shen, L. Bao, Y. Wu, C. Pan, S. Zhao, H. Fang, Y. Xie, P. Jin, P. Peng, F.-F. Li and X. Lu, *J. Am. Chem. Soc.*, 2017, **139**, 9979–9984.
6 X. Zhang, Y. Wang, R. Morales-Martínez, J. Zhong, C. de Graaf, A. Rodríguez-Fortea, J. M. Poblet, L. Echegoyen, L. Feng and N. Chen, *J. Am. Chem. Soc.*, 2018, **140**, 3907–3915.
7 C. Pan, W. Shen, L. Yang, L. Bao, Z. Wei, P. Jin, H. Fang, Y. Xie, T. Akasaka and X. Lu, *Chem. Sci.*, 2019, **10**, 4707–4713.
8 S. Stevenson, G. Rice, T. Glass, K. Harich, F. Cromer, M. R. Jordan, J. Craft, E. Hadju, R. Bible, M. M. Olmstead, K. Maitra, A. J. Fisher, A. L. Balch and H. C. Dorn, *Nature*, 1999, **401**, 55.
9 C.-R. Wang, T. Kai, T. Tomiyama, T. Yoshida, Y. Kobayashi, E. Nishibori, M. Takata, M. Sakata and H. Shinohara, *Angew. Chem., Int. Ed.*, 2001, **40**, 397–399.
10 S. Stevenson, M. A. Mackey, M. A. Stuart, J. P. Phillips, M. L. Easterling, C. J. Chancellor, M. M. Olmstead and A. L. Balch, *J. Am. Chem. Soc.*, 2008, **130**, 11844–11845.
11 L. Dunsch, S. Yang, L. Zhang, A. Svitova, S. Oswald and A. A. Popov, *J. Am. Chem. Soc.*, 2010, **132**, 5413–5421.
12 S. Yang, C. Chen, F. Liu, Y. Xie, F. Li, M. Jiao, M. Suzuki, T. Wei, S. Wang, Z. Chen, X. Lu and T. Akasaka, *Sci. Rep.*, 2013, **3**, 1487.
13 T. Akasaka, S. Nagase, K. Kobayashi, M. Wälchli, K. Yamamoto, H. Funasaka, M. Kako, T. Hoshino and T. Erata, *Angew. Chem., Int. Ed. Engl.*, 1997, **36**, 1643–1645.
14 Y. Yamazaki, K. Nakajima, T. Wakahara, T. Tsuchiya, M. O. Ishitsuka, Y. Maeda, T. Akasaka, M. Waelchli, N. Mizorogi and S. Nagase, *Angew. Chem., Int. Ed.*, 2008, **47**, 7905–7908.
15 T.-S. Wang, N. Chen, J.-F. Xiang, B. Li, J.-Y. Wu, W. Xu, L. Jiang, K. Tan, C.-Y. Shu, X. Lu and C.-R. Wang, *J. Am. Chem. Soc.*, 2009, **131**, 16646–16647.
16 K. Junghans, K. B. Ghiassi, N. A. Samoylova, Q. Deng, M. Rosenkranz, M. M. Olmstead, A. L. Balch and A. A. Popov, *Chem.–Eur. J.*, 2016, **22**, 13098–13107.
17 K. Junghans, C. Schlesier, A. Kostanyan, N. A. Samoylova, Q. Deng, M. Rosenkranz, S. Schiemenz, R. Westerström, T. Greber, B. Büchner and A. A. Popov, *Angew. Chem., Int. Ed.*, 2015, **54**, 13411–13415.
18 M. Krause, F. Ziegs, A. A. Popov and L. Dunsch, *ChemPhysChem*, 2007, **8**, 537–540.
19 T. Wang, J. Wu and Y. Feng, *Dalton Trans.*, 2014, **43**, 16270–16274.
20 Q. Deng, K. Junghans and A. A. Popov, *Theor. Chem. Acc.*, 2015, **134**, 10.
21 X. Zhang, W. Li, L. Feng, X. Chen, A. Hansen, S. Grimme, S. Fortier, D.-C. Sergentu, T. J. Duignan, J. Autschbach, S. Wang, Y. Wang, G. Velkos, A. A. Popov, N. Aghdassi, S. Duhm, X. Li, J. Li, L. Echegoyen, W. H. E. Schwarz and N. Chen, *Nat. Commun.*, 2018, **9**, 2753.
22 A. L. Svitova, K. B. Ghiassi, C. Schlesier, K. Junghans, Y. Zhang, M. M. Olmstead, A. L. Balch, L. Dunsch and A. A. Popov, *Nat. Commun.*, 2014, **5**, 3568.
23 D. Fuchs, H. Rietschel, R. H. Michel, A. Fischer, P. Weis and M. M. Kappes, *J. Phys. Chem.*, 1996, **100**, 725–729.
24 M. Krause and L. Dunsch, *ChemPhysChem*, 2004, **5**, 1445–1449.
25 S. Yang, C. Chen, A. A. Popov, W. Zhang, F. Liu and L. Dunsch, *Chem. Commun.*, 2009, 6391–6393.
26 C. Chen, F. Liu, S. Li, N. Wang, A. A. Popov, M. Jiao, T. Wei, Q. Li, L. Dunsch and S. Yang, *Inorg. Chem.*, 2012, **51**, 3039–3045.

27 K. V. Zaitsev, Y. F. Oprunenko, A. V. Churakov, J. A. K. Howard, S. S. Karlov and G. S. Zaitseva, *J. Organomet. Chem.*, 2008, **693**, 173–179.
28 H. Tsurugi, H. Nagae and K. Mashima, *Chem. Commun.*, 2011, **47**, 5620–5622.
29 R. H. Duncan Lyngdoh, H. F. Schaefer and R. B. King, *Chem. Rev.*, 2018, **118**, 11626–11706.
30 D. Shoken, M. Sharma, M. Botoshansky, M. Tamm and M. S. Eisen, *J. Am. Chem. Soc.*, 2013, **135**, 12592–12595.
31 M. Manßen, N. Lauterbach, J. Dörfler, M. Schmidtmann, W. Saak, S. Doye and R. Beckhaus, *Angew. Chem., Int. Ed.*, 2015, **54**, 4383–4387.
32 Z. Slanina, F. Uhlík, S. Nagase, T. Akasaka, L. Adamowicz and X. Lu, *Molecules*, 2017, **22**, 1053.
33 M. Takata, E. Nishibori, M. Sakata and H. Shinohara, *New Diamond Front. Carbon Technol.*, 2002, **12**, 271–286.
34 W. J. Hehre, *A guide to molecular mechanics and quantum chemical calculations*, Wavefunction, Irvine, CA, 2003.
35 Z. Slanina, F. Uhlík, C. Pan, T. Akasaka, X. Lu and L. Adamowicz, *Chem. Phys. Lett.*, 2018, **710**, 147–149.
36 C. Pan, L. Bao, X. Yu, H. Fang, Y. Xie, T. Akasaka and X. Lu, *ACS Nano*, 2018, **12**, 2065–2069.
37 G. M. Sheldrick, *Acta Crystallogr., Sect. A: Found. Crystallogr.*, 2008, **64**, 112–122.
38 J. S. Binkley, J. A. Pople and W. J. Hehre, *J. Am. Chem. Soc.*, 1980, **102**, 939–947.
39 X. Cao and M. Dolg, *J. Mol. Struct.: THEOCHEM*, 2002, **581**, 139–147.
40 A. D. Becke, *J. Chem. Phys.*, 1993, **98**, 5648–5652.
41 C. Lee, W. Yang and R. G. Parr, *Phys. Rev. B: Condens. Matter Mater. Phys.*, 1988, **37**, 785–789.
42 W. J. Hehre, R. Ditchfield and J. A. Pople, *J. Chem. Phys.*, 1972, **56**, 2257–2261.
43 Z. Slanina, F. Uhlík, S.-L. Lee, L. Adamowicz, T. Akasaka and S. Nagase, *Int. J. Quantum Chem.*, 2011, **111**, 2712–2718.
44 S. F. Boys and F. Bernardi, *Mol. Phys.*, 1970, **19**, 553–566.
45 Z. Slanina, F. Uhlík, X. Lu, T. Akasaka, K. H. Lemke, T. M. Seward, S. Nagase and L. Adamowicz, *Fullerenes, Nanotubes, Carbon Nanostruct.*, 2016, **24**, 1–7.
46 M. J. Frisch, G. W. Trucks, H. B. Schlegel, G. E. Scuseria, M. A. Robb, J. R. Cheeseman, G. Scalmani, V. Barone, B. Mennucci, G. A. Petersson, H. Nakatsuji, M. Caricato, X. Li, H. P. Hratchian, A. F. Izmaylov, J. Bloino, G. Zheng, J. L. Sonnenberg, M. Hada, M. Ehara, K. Toyota, R. Fukuda, J. Hasegawa, M. Ishida, T. Nakajima, Y. Honda, O. Kitao, H. Nakai, T. Vreven, J. A. Montgomery Jr, J. E. Peralta, F. Ogliaro, M. J. Bearpark, J. Heyd, E. N. Brothers, K. N. Kudin, V. N. Staroverov, R. Kobayashi, J. Normand, K. Raghavachari, A. P. Rendell, J. C. Burant, S. S. Iyengar, J. Tomasi, M. Cossi, N. Rega, N. J. Millam, M. Klene, J. E. Knox, J. B. Cross, V. Bakken, C. Adamo, J. Jaramillo, R. Gomperts, R. E. Stratmann, O. Yazyev, A. J. Austin, R. Cammi, C. Pomelli, J. W. Ochterski, R. L. Martin, K. Morokuma, V. G. Zakrzewski, G. A. Voth, P. Salvador, J. J. Dannenberg, S. Dapprich, A. D. Daniels, Ö. Farkas, J. B. Foresman, J. V. Ortiz, J. Cioslowski and D. J. Fox, *Gaussian 09*, Gaussian, Inc., Wallingford, CT, USA, 2009.